Heterocycles form one of the most important and well investigated classes of organic compounds owing to their occurrence in living organisms and showing a wide range of biological activity.

Imidazo[1,2-*a*]pyridines or 1-azaindolizines (**9**) have received significant attention from the pharmaceutical industry owing to their interesting biological activities displayed over a broad range of therapeutic classes, showing antiulcer, antiviral, antifungal and anti-inflammatory activities.

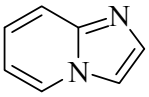

9

Like indolizine, imidazo[1,2-*a*]pyridine is composed of a π-excessive five-membered ring and a π-deficient pyridine ring with only one bridgehead nitrogen. Literature survey reveals that though a number of [8+2] cycloaddition reactions of indolizine with a variety of alkenes and alkynes have been accomplished successfully, no [2+4] cycloaddition has been reported so far. In contrast to indolizine, the reactivity of imidazo[1,2-*a*]pyridine has been investigated experimentally or theoretically sparsely.

With this background, the present study is aimed on the theoretical and experimental investigations of the cycloaddition reactions of imidazo[1,2-*a*]pyridines and their derivatives.

The results of the present investigations have been presented in the following chapters:

Chapter 1. [8+2] Cycloaddition Reactions of Nitrogen Heterocycles: A Review

Chapter 2. Reaction of Imidazo[1,2-*a*]pyridine with Dimethyl Acetylenedicarboxylate: Experimental and Theoretical Results

Chapter 3. Charge-transfer Complexes of Imidazo[1,2-*a*]pyridines with Dimethyl Acetylenedicarboxylate: Experimental and Theoretical Results

Chapter 4. Tuning of Dienophilic Reactivity of Imidazo[1,2-*a*]pyridines: Theoretical and Experimental Results

Chapter 1. [8+2] Cycloaddition Reactions of Nitrogen Heterocycles: A Review

First chapter deals with the experimental and theoretical investigations of the [8+2] cycloadditions of the nitrogen heterocycles right from the beginning to the most recent ones. For the purpose of discussion, it has been classified on the basis of the substrate i.e. number of nitrogen atoms present in the 8π heterocyclic system. Wherever possible, the relevant mechanism, concerted or stepwise, has also been described. The review is divided into three subsections.

1.4.1. [8+2] Cycloadditions of monoazaheterocycles

[8+2] Cycloaddition reactions of monoazaheterocycles namely, indolizines (**8**) and their derivatives, benzannelated indolizines, azaheptafulvenes (**7**), azafulvenium methides (**131**), dienylazaisobenzofurans (**149**) with the appropriate dienophiles, such as dialkyl maleates, alkyl acrylates, DMAD, benzyne, methyl vinyl ketone, methyl propiolate and ethyl propiolate have been compiled in this section.

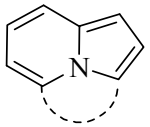

8

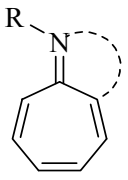

7

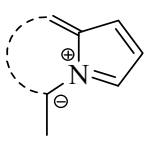

131

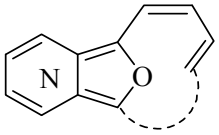

149

1.4.2. [8+2] Cycloadditions of diazaheterocycles

This section includes description of the [8+2] cycloadditions of diazaheterocycles namely, azaindolizines (**9**) with DMAD and benzyne. It also includes [8+2] cycloadditions of diazafulvenium methides with electron-rich and electron-deficient dipolarophiles.

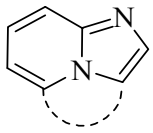

9

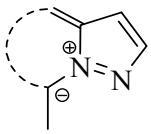

171

1.4.3. [8+2] Cycloadditions of triazaheterocycles

In this section, [8+2] cycloaddition reaction of imidazo[1,2-*a*]pyrimidine with benzyne is discussed.

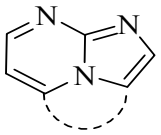

190

Chapter 2. Reaction of Imidazo[1,2-*a*]pyridines with Dimethyl Acetylenedicarboxylate: Experimental and Theoretical Results

This chapter comprises the results of the reaction of imidazo[1,2-*a*]pyridine with DMAD in the absence of dehydrogenating catalyst in different solvents. The mechanism of the reaction has been studied at the DFT [B3LYP/6-31+G(d)] level and formation of different products has been explained on the basis of theoretical calculations. The chapter is divided into following subsections:

2.2. Experimental Results

2.2.1. Synthesis of 2-phenylimidazo[1,2-*a*]pyridine

Appropriately 2-substituted imidazo[1,2-*a*]pyridine derivatives were prepared for the [8+2] cycloaddition reactions. Under microwave irradiation, 2-aminopyridine

(**5**) reacted with *α*-bromoacetophenone (**6**) in the presence of basic alumina to afford 2-phenylimidazo[1,2-*a*]pyridine (**7**) (**Scheme 2.2**).

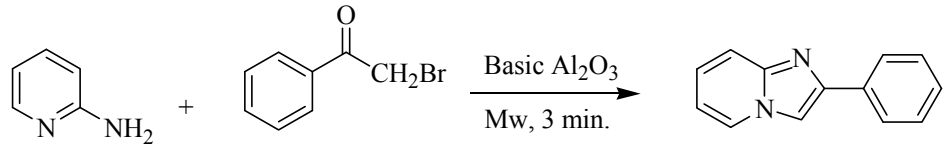

5 **6** **7**

Scheme 2.2. Reaction of 2-aminopyridine (**5**) with *α*-bromoacetophenone (**6**)

A light yellow crystalline product with sharp melting point was obtained. It is readily soluble in polar solvents, such as acetonitrile, methylene chloride and chloroform but dissolves sparingly in non-polar solvents, such as toluene and hexane. It is stable for long duration under inert atmosphere, but decomposes on exposure to air or moisture. The structure of **7** has been established on the basis of IR, ^{1}H NMR and ^{13}C NMR spectral data.

2.2.2. Reaction of 2-phenylimidazo[1,2-*a*]pyridine in methylene chloride

A two-component reaction of 2-phenylimidazo[1,2-*a*]pyridine (**7**) with DMAD (**8**) in methylene chloride gave a complex mixture, from which a Michael adduct (**9**) could be isolated in about 30% quantity (**Scheme 2.3**). No [8+2] cycloadduct was formed, possibly due to the absence of a dehydrogenating agent.

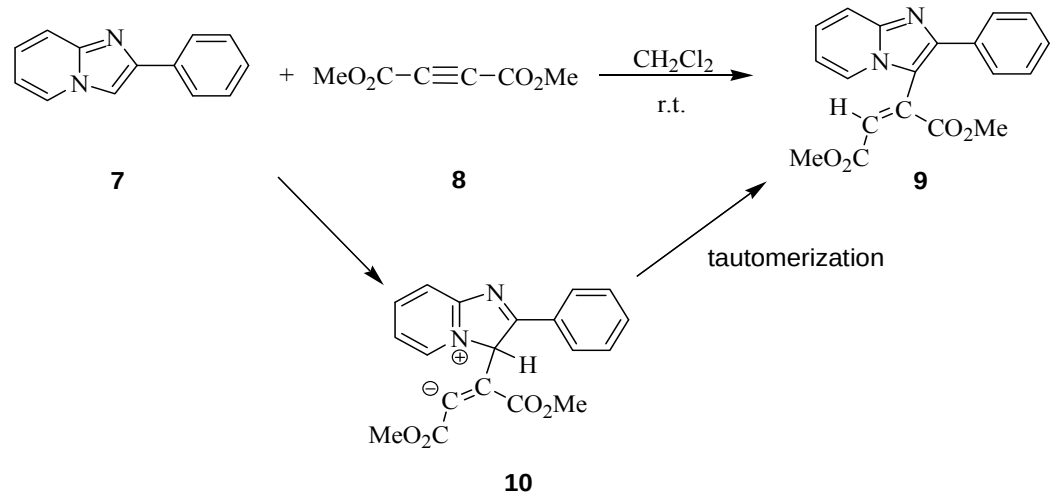

7 **8** **9**

10

Scheme 2.3. Reaction of 2-phenylimidazo[1,2-*a*]pyridine (**7**) with DMAD (**8**)

2.2.2.1. Characterization of the Michael adduct (9)

A pale yellow solid was obtained which was stable under inert atmosphere for prolonged duration but decomposed on exposure to atmosphere. The structure of the compound was established on the basis of spectroscopic techniques (IR, ^{1}H NMR and ^{13}C NMR).

2.2.3. Multicomponent reaction of 2-phenylimidazo[1,2-*a*]pyridine in water

In this section, [8+2] cycloaddition reaction of *in situ* generated 2-phenylimidazo[1,2-*a*]pyridine with DMAD in water has been discussed. It is the first example of a metal free preparation of 1-azacycl[3.2.2]azine.

A three component reaction of 2-aminopyridine (**5**), *α*-bromoacetophenone (**6**) and DMAD (**8**) was accomplished in water in the presence of potassium carbonate to give 1-azacycl[3.2.2]azine (**11**) (**Scheme 2.4**).

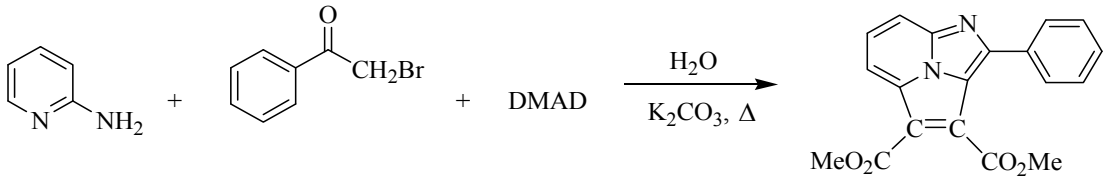

5 **6** **8** **11**

Scheme 2.4. Three component reaction of 2-aminopyridine (**5**), *α*-bromoacetophenone (**6**) and DMAD (**8**)

2.2.3.1. Characterization of 2-phenyl-4,5-bis(methoxycarbonyl)-1-azacycl[3.2.2] azine (11)

Product is white crystalline solid with sharp melting point. It is readily soluble in polar solvents, like acetonitrile, methylene chloride and chloroform but dissolves sparingly in non-polar solvents, like toluene and hexane. It is stable under inert atmosphere for a long period but decomposes on exposure to environment. The

structure of **11** has been confirmed by spectroscopic techniques (IR, ^{1}H NMR and ^{13}C NMR).

2.3. Theoretical Investigation of the Reaction of Imidazo[1,2-*a*] pyridine with DMAD: A Stepwise Mechanism

To investigate the mechanism of the reaction between imidazo[1,2-*a*]pyridines (**7a,b**) with DMAD (**8**), following model reactions have been investigated computationally in the gas phase and in solvent (CH_2Cl_2 and H_2O) at the DFT [B3LYP/6-31+G(d)] level (**Scheme 2.6**).

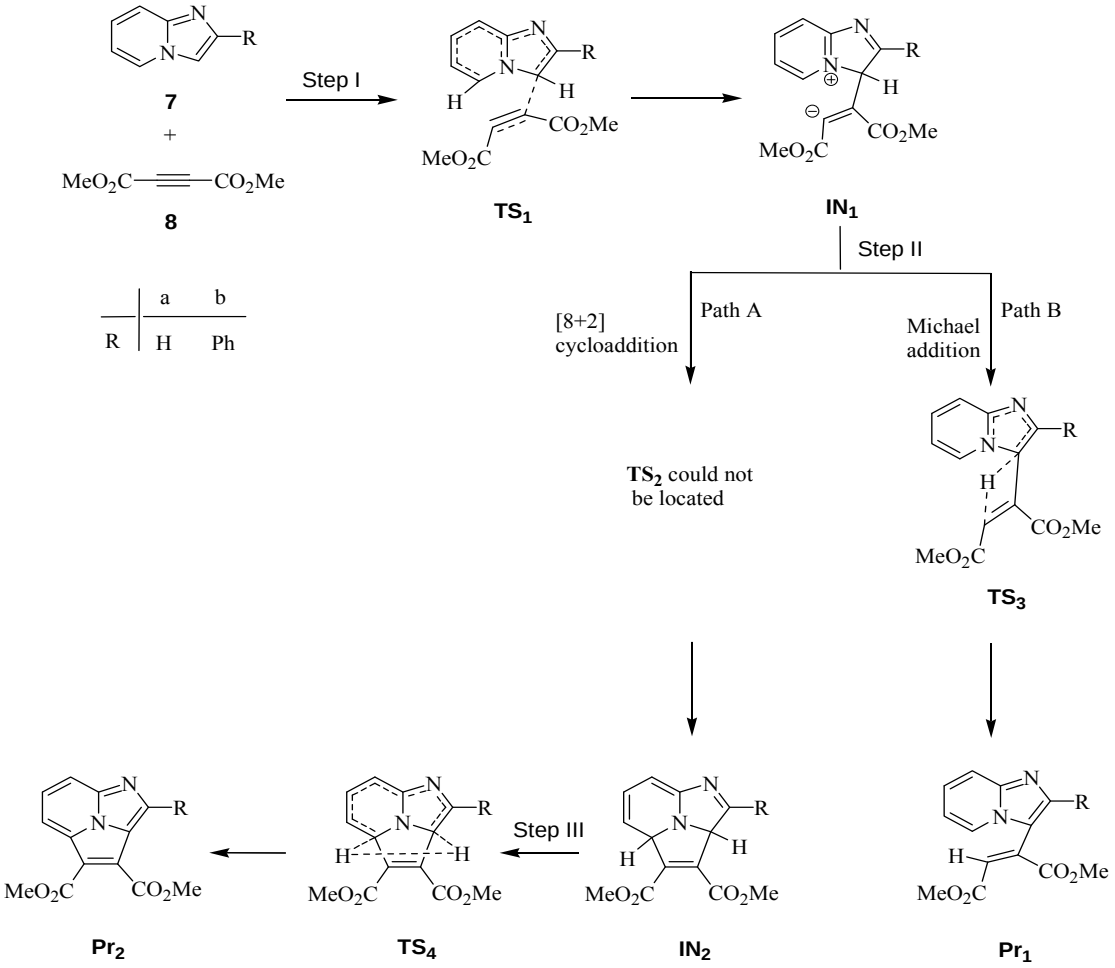

Scheme 2.6. Theoretical investigation of the reaction of imidazo[1,2-*a*]pyridines (**7a,b**) with DMAD (**8**)

2.3.1. Computational details

Various computational techniques and supporting software used during the investigations have been described in this section.

2.3.2. Results and discussion

This section incorporates the optimized geometries [B3LYP/6-31+G(d) level] of the stationary points i.e. reactants, transition structures, intermediates and products in the above reactions. Selected bond distances and the respective Wiberg bond indices (WBI) of these species are given in Table 2.4.

2.3.2.1. Step I: Formation of the intermediate (IN1)

On scanning the potential energy surface (PES), it is found that the above computed reaction proceeds via a stepwise mechanism. The initial reaction involves the nucleophilic attack of C3 of the π-excessive pyrrole ring of imidazo[1,2-*a*]pyridine on the C≡C bond of DMAD leading to the formation of a zwitterionic intermediate $\mathbf{IN_1}$ via a transition structure $\mathbf{TS_1}$. The initial attack of C3 of **7** at DMAD has also been confirmed from the nucleophilicity indices values. The values of global and local reactivity descriptors f_k^- and N_k^- on various atoms of imidazo[1,2-*a*]pyridines are given in Table 2.6. As evinced from the local nucleophilic indices values, C3 site is more nucleophilic than C5 site and the initial attack therefore occurs through C3 of imidazo[1,2-*a*]pyridines. The energies of activation associated with $\mathbf{TS_{1a}}$ and $\mathbf{TS_{1b}}$ are 21.05 and 21.99 kcal mol^{-1}, respectively. It may be noted that in the presence of methylene chloride and water (solvent phase), the activation barrier and exothermicity decrease ranging between 0.24 and 3.51 kcal mol^{-1} and 1.50 and 5.73 kcal mol^{-1}, respectively.

The formation of the C3-C10 bond is more advanced in the case of **TS_{1b}** in comparison to the **TS_{1a}** as indicated by the bond lengths (1.883 Å in **TS_{1b}** and 1.899 Å in **TS_{1a}**) and WBI (0.55 in **TS_{1b}** and 0.53 in **TS_{1a}**), respectively. In zwitterionic intermediates, **IN_{1a}** and **IN_{1b}** the C3-C10 bond lengths are 1.537 (WBI = 0.96) and 1.534 Å (WBI = 0.97), respectively indicating complete formation of a single bond. The lowering in energy of intermediate **IN_{1b}** in comparison to **IN_{1a}** (5.00 kcal mol^{-1}) may be attributed to electronic interaction between the electron pair located in the sp^2 lobe at C11 and delocalization of the positive charge of the pyrrole ring due to the phenyl ring.

The total energies of all the reactants, transition structures and corresponding adducts and relative activation energies (ΔE_a) and energies of reaction (ΔE_{rxn}) of the studied model systems obtained in the gas phase and in solvent (CH_2Cl_2 and H_2O) phase are given in Table 2.7 and 2.8, respectively.

2.3.2.2. Step II: Two paths

The intermediate **IN_1** can undergo further transformations via two different paths:

Path A: Ring closure- Formation of the intermediate (IN_2)

The intramolecular nucleophilic attack of the anionic C11 centre at C5 of the pyridine ring in **IN_1** leads to the ring closure generating **IN_2**. This step appears to be barrierless as all attempts to locate the second transition structure by IRC calculations failed. Instead, the final product is obtained. The overall process is exothermic (-5.80 kcal mol^{-1}). In the cycloadducts, lone pair of the central nitrogen atom interacts strongly with π^*C8-C9 orbital, as indicated by high second-order perturbative energy (~26-29 kcal mol^{-1}).

Path B: Intramolecular H-Transfer- Formation of the Michael adduct

The intermediate **IN_1** undergoes an alternative process, via concerted asynchronous transition state (**TS_3**) leading to the formation of the Michael adduct (**Pr_1**). This process corresponds to intramolecular proton transfer from C3 atom to the anionic C11 centre accompanied by aromatization of the pyrrole ring. It is interesting to note that a *cis* Michael adduct is formed. The formation of *trans* product is ruled out on the basis of the fact that the conversion of initially formed *cis* intermediate into *trans* has to overcome high energy barrier. FMO analysis of the **IN_1** also supports the formation of *cis* product. It is found that the HOMO, which is a π-orbital, encompasses C3C10C11 moiety, thus restricting the rotation about the C10-C11 bond. The activation energy barrier for this step is quite high (31.54 kcal mol^{-1} for **TS_{3a}** and 29.31 kcal mol^{-1} for **TS_{3b}**). This transition structure (**TS_3**) corresponds to a four-membered structure. Due to this, angular strain is present, which raises the activation barrier. However, the resulting Michael adduct is thermodynamically very stable (-41.16 kcal mol^{-1} for **Pr_{1a}** and -36.08 kcal mol^{-1} for **Pr_{1b}**).

2.3.2.3. Step III: Oxidation of IN_2 to [8+2] cycloadduct

The intermediate **IN_2** formed in the second step is unstable and gets oxidized to give aromatized compound (**Pr_2**), after loss of hydrogen. Overall reaction is exothermic with high activation barrier i.e. 45 kcal mol^{-1} for reaction 1 while the analogous energy barrier for the reaction 2 is lower by ~1 kcal mol^{-1}. The aromatization of the imidazo and pyridine rings of **IN_{2a}** and **IN_{2b}** appears to be the main driving force for this reaction. Experimentally, there might be possibility of auto-oxidation by which hydrogen departure takes place.

Both $\mathbf{TS_{4a}}$ and $\mathbf{TS_{4b}}$ have large negative values of NICS(0); however, NICS(1) values are lower. These results confirm that these TSs are aromatic in nature. This indicates concerted cleavage of C3-H3 and C5-H5, which generates a strong diamagnetic ring current along the imidazo[1,2-*a*]pyridine ring and new forming five-membered ring.

2.4. Experimental Details

Various procedures and experimental techniques used during the synthesis of 2-phenylimidazo[1,2-*a*]pyridine and its [8+2] cycloadduct and Michael adduct formation are given in this section.

2.5. Conclusions

From experimental and computational studies of the reaction between imidazo[1,2-*a*]pyridines with DMAD, it can be concluded that: (i) the reaction may follow one of the two alternative paths leading to [8+2] cycloaddition or Michael addition. (ii) The reaction occurs via a stepwise manner due to the presence of the ester groups as a result of which charge delocalization occurs effectively; this step is the rate determining step. (iv) Michael adduct is thermodynamically preferred, while [8+2] cycloadduct is kinetically preferred. (iv) It appears that the nature of the solvent and conditions of the reaction play important role in determining the course of the reaction. In dichloromethane, at room temperature (~25 ºC), Michael adduct (30%) is formed, while reaction in water at elevated temperature affords [8+2] cycloadduct.

Chapter 3. Charge-transfer Complexes of Imidazo[1,2-*a*]pyridines with Dimethyl Acetylenedicarboxylate: Experimental and Theoretical Results

3.1. Introduction

The interest in the study of the CT-complexes resulting from the interaction of σ- and π-electron-acceptors with organic π- and n-electron-donors increased much recently owing to their significant physical and chemical properties, both in the solid state and in solution. CT-complexes have diverse applications.

3.2. Charge-transfer Complexes of Pyridines and Annelated Pyridines- A Review

As our investigated compounds, namely imidazo[1,2-*a*]pyridines belong to the general class of pyridines and annelated pyridines, this review comprises the CT-complexes of this class of compounds only due to space-constraint. Also, the present review is restricted to the literature covering the last decade, i.e. from the year 2005 through 2015. Methods of the preparation of the CT-complex of the pyridine donors, their characterization and structural studies are discussed in this section. For the identification of the CT-complex formation, most widely used method is electronic spectroscopy, particularly the UV-visible absorption spectroscopy. In many cases, CT-complexes were obtained in solid state and their structures were determined by IR, ^{1}H NMR and mass spectral techniques and also by X-ray crystal analysis. In a few cases, thermogravimetric analysis and fluorescence spectra have been studied. A number of reports deal with the theoretical investigation of these CT-complexes. Review also includes briefly applications of the CT-complexes.

While studying [8+2] cycloaddition of imidazo[1,2-*a*]pyridine, (imdpy) with DMAD, we noticed that on adding the solution of DMAD to a solution of imdpy, pink color developed with high exothermicity. These observations motivated us to investigate the CT-complexes of a few representative imidazo[1,2-*a*]pyridines with DMAD experimentally and theoretically. The results are presented in the following subsections:

3.3. Experimental Details

Various procedures and experimental techniques used during the investigation of the CT-complexes of differently substituted imidazo[1,2-*a*]pyridines are given in this section.

3.4. Computational Details

The methods of the computational calculations and details of the supporting software used during the investigations are described in this section.

3.5. Results and Discussion

3.5.1. Experimental results

3.5.1.1. Electronic absorption spectra

In this section, electronic absorption spectra of donor, acceptor and respective CT-complex are discussed. The absorbance spectra of the CT-complexes exhibit new absorption bands at a longer wavelength than the donors (λ_{max} < 350 nm) or the acceptor (λ_{max} < 230 nm) alone. It is observed that with the change in the substituent group, molar absorptivity changes. The decrease in ε is in the order H > OMe > Ph > F > NO_2.

The interaction between imidazo[1,2-*a*]pyridines (**69a-e**) and DMAD (**70**) involves π→π* transition forming radical-ion pairs, i.e. radical-cation and radical-anion pairs, **71a-e** (**Scheme 3.18**).

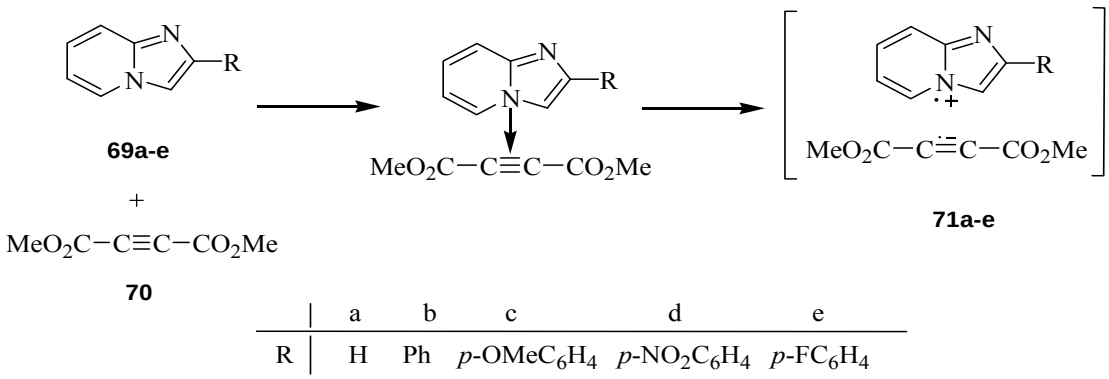

Scheme 3.18. CT-complexation between imidazo[1,2-*a*]pyridines (**69a-e**) and DMAD (**70**)

It is noteworthy that substitution at the 2-position of imidazo[1,2-*a*]pyridine by phenyl or *p*-substituted phenyl group is accompanied by a hypsochromic shift of 4-30 nm and decrease in the molar absorptivity. A hypsochromic shift can be correlated with an increased energy for the π–π* transition, whereas a decrease in the molar absorptivity can be attributed to reduced density of the negative charge at the 3-position of the donor. It may be noted that the E_{CT} values of the CT-complexes accord well with the observed λ_{max} values of the CT-complexes: **71a** with the smallest E_{CT} value absorbs at the longest λ (510 nm), whereas **71d** with the highest E_{CT} value absorbs at the shortest λ (480 nm). Similarly, **71a** having largest value of the molar absorptivity has highest negative charge density at the 3-position. In fact, these structural changes result due to the –I (inductive) effect of the phenyl or *p*-substituted phenyl group.

3.5.1.2. Spectrophotometric titration measurements

Spectrophotometric titration measurements were done to determine the reactions' stoichiometries which are discussed in this section. It is seen from the photometric titration curves that absorbance of the CT-complex increases with increasing the concentration of imidazo[1,2-*a*]pyridine, but after 1:1 stoichiometry, it becomes nearly constant. So, the results confirm a reaction stoichiometry of 1:1 of the CT-complexes formed between the donor and DMAD. So, the complex could be formulated as [(imidazo[1,2-*a*]pyridine)(DMAD)].

3.5.1.3. Formation constant (K_{CT}) and molar extinction coefficient (ε_{CT}) of the CT-complexes

The spectrophotometric data were used to calculate values of the equilibrium constants, K_{CT} and the molar extinction coefficients, ε of the CT-complexes in CH_2Cl_2 for **71a-e** having 1:1 stoichiometries using the modified Benesi-Hildebrand equation. A high value of the formation constant, K_{CT} reflects higher stability of the formed CT-complex, which depends strongly on the nature of the donor. Thus a higher value of the K_{CT} of the CT-complex formed by unsubstituted imidazo[1,2-*a*]pyridine (**69a**) implies its higher stability, which decreases in the order **69a > 69c > 69b > 69e > 69d**.

3.5.2. Theoretical results

To understand the energetics of the mechanism of the CT-complexation, a model reaction of imidazo[1,2-*a*]pyridine (**69a**) with DMAD (**70**) was investigated theoretically at the M06 and B3LYP functionals using 6-31++G(d,p) basis set. The results obtained are presented in the subsequent sections.

3.5.2.1. Ground state optimization in the gas phase

The optimized geometries of imidazo[1,2-*a*]pyridine (**69a**), DMAD (**70**) and the resulting CT-complex (**71a**) are presented in this section. The structural parameters of the ground state optimized geometries obtained at the M06 and B3LYP levels are also summarized in this section.

It was found that the results obtained from the calculations done at the B3LYP/6-31++G(d,p) level approached the experimental values more closely than those obtained with the M06 functional.

3.5.2.2. Determination of the CT-transition energy in the gas phase

TDDFT calculations using four functionals, namely, M06, B3LYP, CAM-B3LYP, LC-BLYP were carried out and the results obtained are given in this section. The transition energy, $h\nu_{CT}$ of the CT-complex obtained theoretically in the gas phase at the B3LYP/6-31++G(d,p) level is 3.09 eV. In comparison to the theoretically calculated value, the experimental value is significantly low (2.43 eV) which may be on account of the solvent effect.

3.5.2.3. Study of the FMOs of the CT-complex

The FMOs of the CT-complex obtained at the B3LYP/6-31++G(d,p) level are discussed in this section. It shows that upon photo-excitation, electron transfer is feasible from the imdpy to the DMAD moiety in the CT-complex. It is also seen that there is electrostatic interaction between imdpy and DMAD in the gas phase.

3.6. Conclusions

From the above studies, it can be concluded that imidazo[1,2-*a*]pyridine and DMAD form a pink coloured 1:1 CT-complex exhibiting maximum absorption at λ

510 nm. Substitution at the 2-position of imidazo[1,2-*a*]pyridine by phenyl or *p*-substituted phenyl group causes a small hypsochromic shift with slight lowering of the molecular absorptivity (ε_{CT}), which can be rationalized on the basis of the charge-transfer transition energy (E_{CT}) and density of the negative charge at the donor site.

TDDFT calculations with B3LYP functional using 6-31++G(d,p) basis set confirm charge-transfer from imidazo[1,2-*a*]pyridine to DMAD. Furthermore, these calculations reveal that the two molecules acquire almost parallel orientation in the CT-complex which makes the charge-transfer from donor to the acceptor possible. TDDFT calculations with B3LYP functional give much better results than the M06 functional.

Chapter 4. Tuning of Dienophilic Reactivity of Imidazo[1,2-*a*] pyridines: Theoretical and Experimental Results

This chapter comprises results of the theoretical investigation of tuning dienophilic reactivity of imidazo[1,2-*a*]pyridines and also the experimental results of the reaction of imidazo[1,2-*a*]pyridine with tetrachloro-*o*-benzoquinone. The results are presented in the following subsections:

4.3. Computational Details

The methods of the computational calculations and details of the supporting software used during the investigations have been described in this section.

4.4. Results and Discussion

4.4.1. Theoretical results

4.4.1.1. Normal Electron Demand Diels-Alder reactions

The DA reactions of unsubstituted imidazo[1,2-*a*]pyridine (**1a**) and its derivatives (**1b-j**) with 1,3-butadiene have been computed at the B3LYP and B3LYP-D levels. **(Scheme 4.1)**.

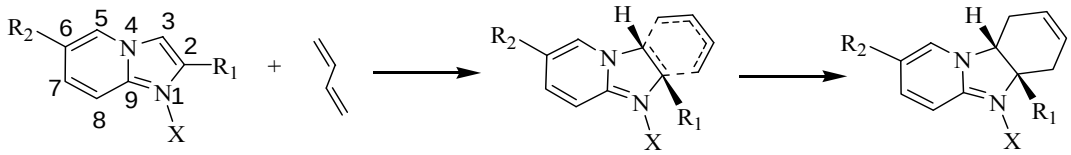

1_{a-j} **2** **TS_{a-j}** **Pr_{a-j}**

Reaction No.	**1**	**2**	**3**	**4**	**5**	**6**	**7**	**8**	**9**	**10**
Species	**a**	**b**	**c**	**d**	**e**	**f**	**g**	**h**	**i**	**j**
R^1	H	CF_3	CH_3	NO_2	H	H	H	H	H	H
R^2	H	H	H	H	CF_3	CH_3	NO_2	H	NO_2	H
X	-	-	-	-	-	-	-	$AlCl_3$	$AlCl_3$	CH_3

Scheme 4.1. Theoretically investigated NED DA reactions

4.4.1.1.1. Optimized geometries

a) In gas phase

The optimized geometries of the stationary points for NED DA reactions (1-10) of differently substituted imidazo[1,2-*a*]pyridines with 1,3-butadiene are presented in this section. The change in the relevant structural parameters are also described.

The global electrophilicity (ω) of the two addends involved in the cycloaddition predicts the imidazo[1,2-*a*]pyridines (**1a-j**) to be acting as electrophile while 1,3-butadiene (**2**) as nucleophile. Thus, this reaction corresponds to the normal electron demand (NED) category of cycloadditions. All the NED DA reactions are

found to follow pericyclic mechanism and involve a concerted but asynchronous transition state. The formation of C10-C3 bond (WBI ~0.38-0.74) is much ahead of C13-C2 bond (WBI ~0.12-0.38). It can be well understood on the basis of electrophilicity indices of C3 and C2 atoms of imidazo[1,2-*a*]pyridines (**1a-j**) (**Table 4.3**). From local electrophilicity values, it is clear that C3 is more electrophilic than C2. The asynchronicity is highest in the TS (WBI = 0.68, 0.12) resulting from **1d** having -NO_2 at the 2-position. It is interesting to find that asynchronicity is very small [in $\mathbf{TS_h}$ (WBI = 0.43, 0.37) and $\mathbf{TS_i}$ (WBI = 0.42, 0.36)] or almost negligible [in $\mathbf{TS_j}$ (WBI = 0.39, 0.38)] in the transition states resulting from the DA reactions of **1h-j**. This can be explained on the basis of the torsional angle (Dh C10C11C12C13) in **TSs** of different reactions, wherein torsional angle varies from ~9.0º to ~0.0º resulting into the change in asynchronicity from high to low (**Table 4.4**). It is found that in B3LYP-D method (B3LYP functional with dispersion correction), the transition states are reached somewhat earlier, as may be expected from the greater exothermicities of the reactions in this case.

Almost equal bond lengths and WBI of three C-C bonds of the diene moiety and partial double bond character of the CC moiety of newly formed six-membered ring accompanied by the delocalization of electrons confer aromatic character on the transition states.

b) In solution

The effect of solvent on geometry relaxation was examined in dichloromethane. For this purpose, geometries of all the species were fully optimized in dichloromethane at the B3LYP level.

In reactant **1a**, the increased contribution of the polar resonance structure **1a′** is manifested by lengthening of the N1-C9 bond with a concurrent shortening of the N4-C9 bond. In the transition structure $\mathbf{TS_{a'}}$, another factor, namely distortion of the planarity of the five-membered ring comes into play and relaxation of the geometry in dichloromethane is revealed by the smaller change in the torsional angles C9-N1-C2-C3 and N4-C3-C2-N1 than those in the gas phase (**Figure 4.8**).

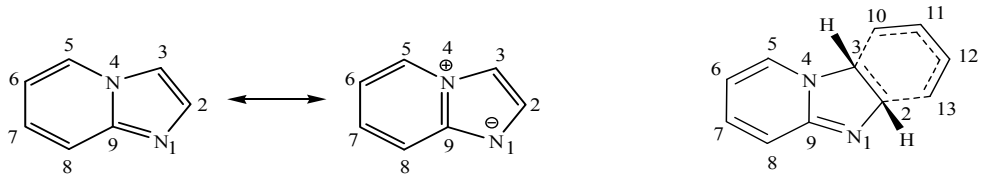

1a **1a′** $\mathbf{TS_a}$

N1-C9 =1.333 (1.336) N1-C9 =1.336 (1.343)
N4-C9 = 1.410 (1.408) N4-C9 = 1.401 (1.396)
Dh C9-N1-C2-C3 = 0.00 (0.00) Dh C9-N1-C2-C3 = 2.72 (2.68)
Dh N4-C3-C2-N1 = 0.00 (0.00) Dh N4-C3-C2-N1 = -8.93 (-8.76)

Figure 4.8. The selected bond lengths (in Å) and torsional angles (in deg.) in **1a** and $\mathbf{TS_a}$ obtained using B3LYP level in gas phase and in dichloromethane (in parentheses)

4.4.1.1.2. Energetics

This section includes total energies, relative activation energies (ΔE_a) and the energies of reactions (ΔE_{rxn}) for the NED DA reactions, 1-10.

It is found that there is a remarkable effect of the dispersion correction on the energy profile. Dispersion effect causes stabilization of the transition structure $\mathbf{TS_a}$ by as much as 10.42 kcal mol^{-1}, as compared to the TS obtained without taking dispersion effect into consideration. Likewise, the product is also stabilized on account of dispersion effect by 9.47 kcal mol^{-1}. Analogously, substituted imidazo[1,2-*a*]pyridines also exhibit decrease in the activation barrier by ~10-13 kcal mol^{-1} and increase in exothermicity of the reactions by ~9-13 kcal mol^{-1} when the computations are done including dispersion effect. It is interesting to note that after dispersion

correction, activation barriers of the DA reactions of 2-nitroimidazo[1,2-*a*]pyridine (reaction 4) as of its $AlCl_3$ complex and N1-methylated derivative (reactions 9-10) lie in the range of 17-19 kcal mol^{-1} only, which indicates the possibility of their occurrence.

Energetics in solution

The effect of the solvent-induced geometry relaxation on the relative free energy of solvation was examined in dichloromethane. It is found that all the species including the transition states are more stable in dichloromethane than in the gas phase and the presence of a substituent group such as NO_2 or coordination of N1 to $AlCl_3$ increases the magnitude of the relative free energy of solvation further. In the case of N1-methylated species (j), which is ionic in nature, this effect is remarkably high.

In the solvent, the transition state is stabilized to a greater extent than the corresponding reactant, and therefore, the overall relative activation energy in dichloromethane is lower than in the gas phase. Similarly, in the solvent, as the product is stabilized more than the reactant, the overall relative reaction energy is greater than in the gas phase.

4.4.1.1.3. NBO analysis

Strong second-order perturbative interaction nN1→π*C2=C3 is noted in the reactant **1d**, making C2=C3 π-bond weaker. Thus, 2-nitroimidazo[1,2-*a*]pyridine is expected to undergo NED DA reaction on C2=C3 functionality.

In all cases, participation of N4 lone pair of electrons in delocalization is evident from the double bond occupancy values which lie in the range of ~1.47e.

However, in **1d, 1i** and **1j,** no electron occupancy could be detected at N4. On the other hand, the lone pair of N1 remains almost unaffected (occupancy~1.92e) except in $AlCl_3$ complexes e.g. **1h and 1i** wherein it is 1.80e. It explains why the use of a Lewis acid such as $AlCl_3$ coordinated through N1 of **1a** and **1g** is not able to reduce the activation barrier significantly; it is lowered by ~3 kcal mol^{-1} only in each case. Furthermore, for methylation (**1j**), N1 still has an occupancy of ~1.52e. This is the reason why methylation of N1 (**1j**) could not induce sufficient electron-deficiency in the five-membered ring.

4.4.1.1.4. FMO analysis

FMO analysis reveals that only the LUMO of 2-nitroimidazo[1,2-*a*]pyridine (**1d**) has appropriate symmetry and sufficiently large coefficients at C2 and C3 to make this compound undergo NED DA reaction.

4.4.1.2. Inverse Electron Demand Diels-Alder reactions

To study the energetics and the mechanism of the IED DA reaction, a model reaction of imidazo[1,2-*a*]pyridine with tetrachloro-*o*-benzoquinone (TCQ), an electron-deficient diene was investigated theoretically at the B3LYP and B3LYP-D levels **(Scheme 4.2)**.

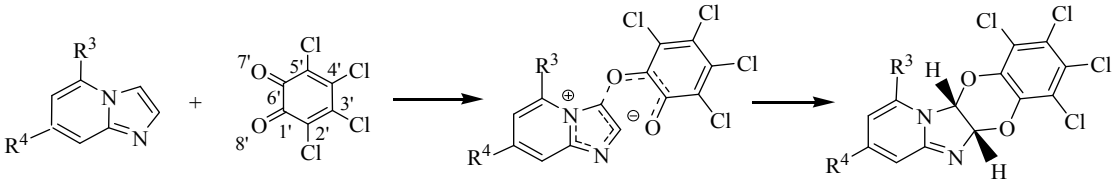

Reaction No.	11	12	13	14
Species	k	l	m	n
R^3	H	NH_2	OMe	H
R^4	H	H	H	NH_2

Scheme 4.2. Theoretically investigated IED DA reactions

4.4.1.2.1. Optimized geometries

a) In gas phase

Optimized geometries of the stationary points and relevant structural parameters of the IED DA reactions are described in this section. The global electrophilicity (ω) of the two addends involved in the cycloaddition predicts the imidazo[1,2-*a*]pyridines (**1a,1l-n**) to be acting as nucleophile while TCQ (**3**) as electrophile. Thus, this reaction corresponds to the inverse electron demand (IED) category of cycloadditions. While exploring the potential energy surface of the DA reaction of **1a** with **3**, it is found that the reaction proceeds via stepwise mechanism. It initiates by the attack of C3 of **1a** on O7' of TCQ, As evinced from the local nucleophilic indices values, it can be seen that C3 site is more nucleophilic than C2 site and the initial attack therefore occurs through C3 of imidazo[1,2-*a*]pyridines. The second step leading to the ring closure, however, appears to be barrierless as the attempts to locate intermediate or the second TS in both methods failed. The IRC calculations do not lead to the intermediate; instead they give the final product. The presence of $–NH_2$ or –OMe group at the 5-position does not change the energetics of the reaction. In these cases also, the reaction occurs via stepwise mechanism with the second step being barrierless.

It is noted from the bond length values that formation of the C3-O10 bond is more advanced in B3LYP-D (1.728-1.744 Å) method in comparison to B3LYP (1.759-1.813 Å) method. As a result, TS in the dispersion corrected method reaches slightly earlier.

b) In solution

The effect of solvent on geometry relaxation was examined in dichloromethane. Geometry relaxation of the transition states ($\mathbf{TS_{k-n}}$) in solution is manifested by shortening of the N4-C9 bond (0.001-0.005 Å) and N1-C2 bond (0.004-0.005 Å) with concurrent lengthening of the N1-C9 bond (0.010-0.012 Å). Furthermore, the torsional angles C9-N1-C2-C3 and N4-C3-C2-N1 in the transition structures experience increase of 0.934-1.703 and decrease of -0.114-1.483 degrees respectively as compared to in the gas phase indicating relaxation of the distorted geometry of the five-membered ring in solution.

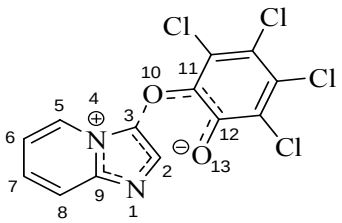

$\mathbf{TS_k}$

N1-C9 = 1.359 (1.370)
N4-C9 = 1.393 (1.388)
Dh C9-N1-C2-C3 = 3.688 (5.084)
Dh N4-C3-C2-N1 = -8.858 (-9.796)

Figure 4.15. The selected bond lengths (in Å) and torsional angles (in degree) in $\mathbf{TS_k}$ in the IED DA reaction obtained at the B3LYP/6-31+G(d,p) level in the gas phase and in dichloromethane (in parentheses)

4.4.1.2.2. Energetics

This section includes total energies, relative activation energies (ΔE_a) and the energies of reactions (ΔE_{rxn}) for the IED DA reactions, 11-14. It may be noted that, as in the case of the NED DA reactions, inclusion of the dispersion correction also lowers the activation barrier of IED DA reactions by ~10 kcal mol^{-1} and increases the exothermicity of the reaction by ~8 kcal mol^{-1}. As expected, the activation energy barrier in the presence of $–NH_2$ or –OMe group at the 5-position, particularly in the

presence of an amino group, is lowered. Interestingly, after dispersion correction, the relative activation barriers for the IED DA reactions of 5-amino- and 7-aminoimidazo[1,2-*a*]pyridines found to be 0.46 kcal mol^{-1} and -0.75 kcal mol^{-1}, respectively indicating the possibility of their immediate occurrence.

Energetics in solution

As expected in this case, due to polar character approaching zwitterionic nature of the transition states, their relative solvation free energies are greater than those of the transition states in the NED DA reactions.

4.4.1.2.3. NBO analysis

NBO analyses of the reactants reveal high second-order perturbative interactions between the nitrogen lone pair (N4) and the π-orbitals which is evident from the double bond occupancy values which lie in the range of ~1.47e. On the other hand, the lone pair of N1 remains almost unaffected (occupancy ~ 1.92e).

Furthermore, presence of lone pair of electrons on C11 in the transition structures is indicated by NLMO occupancy (1.01e). High second-order perturbative interactions between LPC11 to σ*C3-C10 (30.28-53.97 kcal mol^{-1}) and LPC11 to π*C12-O13 (62.12-71.82 kcal mol^{-1}) facilitate stabilization of the transition structure.

The initiation of the formation of an advanced single bond between C3 and C10 can also be noted on the basis of NLMO occupancy (1.84e) of the new forming bond. NLMO occupancy (~1.98e) reveals complete formation of the bond between C3-C10 in the corresponding cycloadducts. NBO studies reveal nil occupancy between C2-O13 in the transition structures. In the corresponding cycloadducts, however, NLMO

occupancy (~1.98e) reveals complete formation of the C2-O13 bond which confirms the stepwise mechanism of the IED DA reaction.

4.4.1.2.4. FMO analysis

An inspection of the FMOs of the reactants shows that the initial contact occurs between C3 of **1a,1l-n** and O7′ of **3**, both centres having FMOs in-phase. In accordance with the IED DA reaction, HOMO of the dienophile (**1a,l-n**) interacts with the LUMO of the electron-deficient diene (**3**). It can be seen that the energy gap between HOMO-LUMO is very small particularly, in the case of 7-aminoimidazo[1,2-*a*]pyridine, which explains lowering of the activation energy barrier in the substituted imidazo[1,2-*a*]pyridines.

4.4.2. Diels-Alder reaction of imidazo[1,2-*a*]pyridine with tetrachloro-*o*-benzoquinone: Experimental results

On reacting imidazo[1,2-*a*]pyridine (**1a**) with tetrachloro-*o*-benzoquinone (**3**) in dichloromethane at room temperature (~30 ^{o}C), a complex mixture of products was obtained, which has been explained on the basis of IR and ^{1}H NMR in this section.
The possible pathways leading to the formation of the products **4** (+**5**) and **7** have been outlined.

The path A involves an ionic mechanism resulting into the formation of [2+4] cycloadduct (**4**), which further aromatizes to yield final product **5.** The formation of the product **7** can be explained on the basis of a free radical mechanism (via path B). The homologous cleavage of a C-C π-bond and C-O π-bond results into the formation of a biradical followed by proton transfer leading to **7**.

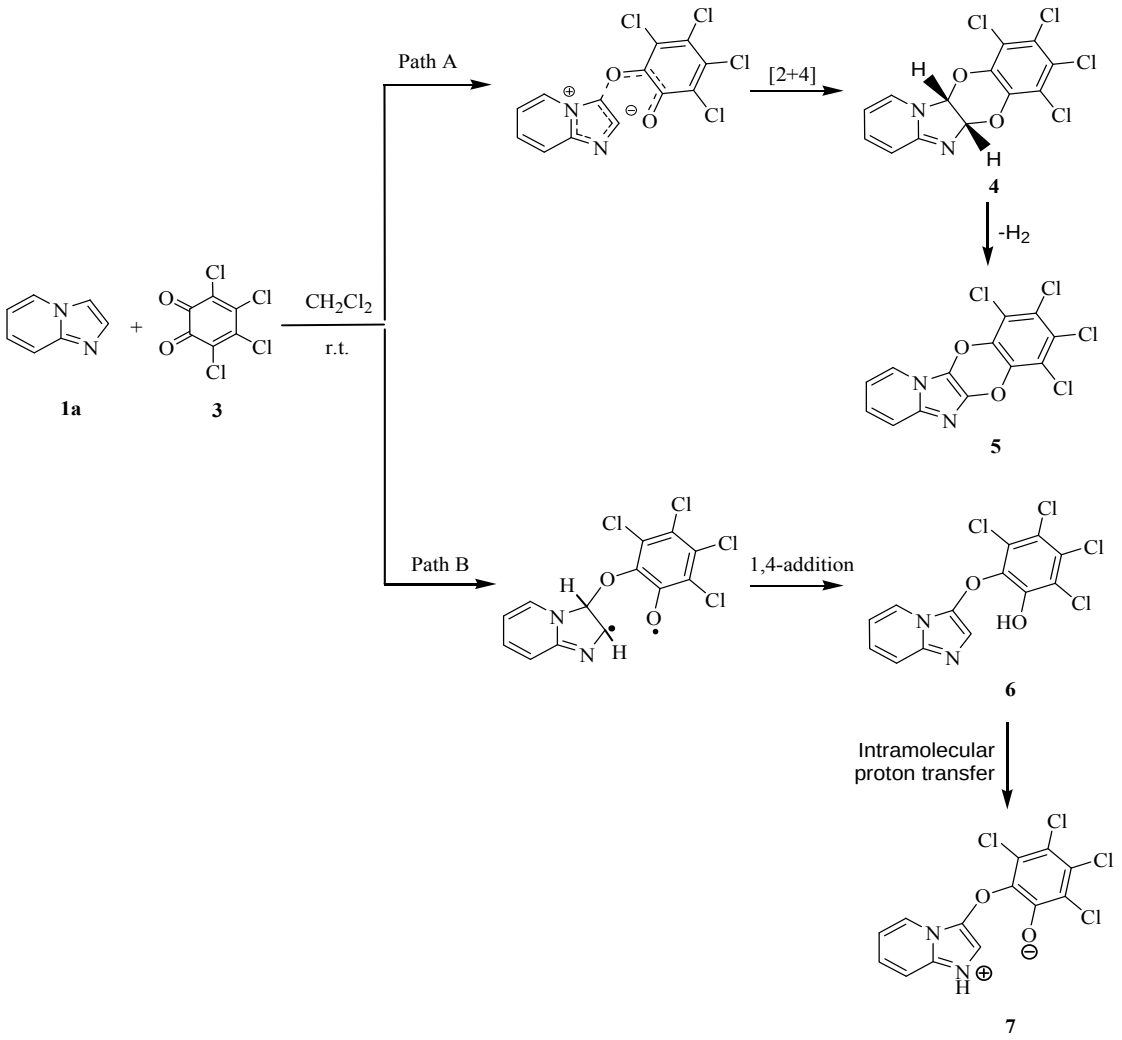

Scheme 4.3. Reaction of imidazo[1,2-*a*]pyridine with TCQ

4.5. Experimental Details

Various procedures and experimental techniques used during the reaction of imidazo[1,2-*a*]pyridine with TCQ are given in this section.

4.6. Conclusions

From computational investigation of the NED DA reaction between imidazo[1,2-*a*]pyridines with 1,3-butadiene, it can be concluded that the relative activation barriers determined by B3LYP/6-31+G(d,p) calculations are higher by ~10-13 kcal mol^{-1} and the relative reaction energies are lower by ~9-13 kcal mol^{-1} than the results obtained by including dispersion correction, although both methods locate

asynchronous concerted transition structures with small deviations in the lengths of the two new forming C-C bonds. A similar trend in the activation barriers and reaction energies is observed in the IED DA reactions of imidazo[1,2-*a*]pyridines with TCQ. However, IED DA reactions proceed by stepwise mechanism and the second step is found to be barrierless. The relative solvation free energies of the reactant and product molecules as well as the transition states in dichloromethane reveal geometry relaxation, as confirmed by the change in the geometric parameters. As expected, the relative solvation free energies of the ionic species are remarkably high. The NED as well as IED DA reactions of imidazo[1,2-*a*]pyridines do not involve reactant- or product-complexes. The reaction of imidazo[1,2-*a*]pyridine with TCQ in dichloromethane at room temperature (~30 ºC) yielded a mixture of products, [4+2] cycloadduct, dihydro-[4+2] cycloadduct and 1,4-addition product, which can be rationalized on the basis of an ionic and biradical stepwise mechanism respectively.

At the end of the thesis, 247 references and supplementary information have been appended.